Egyptian Journal of Radiology and Nuclear Medicine

RESEARCH

Open Access

MRI as a one-stop destination for evaluation of CSF shunt malfunction

Eman Ahmed Hamed[1*], Shaimaa Abdelsattar Mohammad[1], Shrouk M. Awadallah[1], Assem Mounir Metwalli Abdel-Latif[2] and Abeer Maghawry Abd-Elhameed[1]

Abstract

Background Despite the high-frequency rate of cerebrospinal fluid shunt malfunction, radiological evaluation of CSF shunts has remained deficient, focusing mainly on demonstrating secondary signs of shunt failure rather than evaluating the shunt tube itself. We aimed to study the utility of different MR pulse sequences in evaluating the cranial and abdominal ends of CSF shunts in order to identify the potential cause of shunt failure and its impact on patient management.

Results Twenty-five patients (18 males, 7 females, median age 2.5 years, IQR 0.75–15) were enrolled in the study, having 28 ventriculo-peritoneal shunts and single ventriculo-gallbladder shunt. The catheter lumen and fine intraventricular septae were only demonstrated in 3D-DRIVE sequences ($p < 0.001$). Except for three patients (having cranial end-related complications), all patients with cranial and/or abdominal end-related complications received surgery ($p < 0.001$, positive likelihood and negative likelihood ratios = 7.27, 0.3, respectively, sensitivity = 0.7 and specificity = 0.9). MRI findings (luminal occlusion, disconnection, CSF collection, or migration) were consistent with operative data. There is no significant difference between patients who underwent surgery and those with conservative management, or symptomatic and asymptomatic patients in terms of the prevalence of ventricular dilatation or white matter signal abnormality. The results of the abdomino-pelvic fat-suppressed T2-WI showed excellent agreement with ultrasound findings (Cohen's Kappa 0.9). Quantitative PC could give insights into CSF dynamics, which depend on the site and cause of shunt malfunction.

Conclusions MRI could be a one-stop destination for evaluating patients with suspected non-acute shunt malfunction. It was found to have clinical relevance in terms of accurately locating the exact site and possible cause of shunt-related complications.

Keywords CSF shunt malfunction, Hydrocephalus, Ventriculo-peritoneal shunts, Ventriculo-gallbladder shunts

Background

Cerebrospinal fluid (CSF) shunting is the standard treatment of hydrocephalus [1–3]. Ventriculo-peritoneal shunt (VP) is the mainstay for CSF diversion [4–6]. However, despite the progress in management and the advances in shunt hardware design, malfunction rates continue to be disappointingly high [7, 8]. CSF shunt malfunction is a potential life-threatening condition if goes unrecognized and thus it requires instantaneous diagnosis and prompt management [9, 10].

Unenhanced CT has been used for the evaluation of CSF shunts in the emergency setting [8, 10–12]. Rapid

*Correspondence:
Eman Ahmed Hamed
ea531584@gmail.com; eman_hamed@med.asu.edu.eg
[1] Department of Diagnostic and Interventional Radiology, and Molecular Imaging, Faculty of Medicine, Ain Shams University, Ramsis St., Abbasia, Cairo 11657, Egypt
[2] Department of Neurosurgery, Faculty of Medicine, Ain Shams University, Ramsis St., Abbasia, Cairo 11657, Egypt

MRI brain protocols using single-shot fast T2 sequences have been employed for shunt assessment without risk of sedation or radiation exposure. Both CT and rapid MRI protocols have been focusing mainly on demonstration of ventricular system dilatation, visualization of ventricular configuration, transependymal CSF permeation, and catheter localization. However, visualization of the catheter lumen remained problematic [13–15].

Newly developed high-resolution heavily T2-weighted volumetric sequences (e.g., three-dimensional driven equilibrium 3D-DRIVE) have been recently added to the MR protocol for imaging of hydrocephalus [16–18]. The high-resolution sequences are superior to conventional MR protocol in the assessment of subarachnoid space and demonstration of thin obstructive membranes [17, 18].

Correct recognition of shunt failure is challenging. Moreover, the exact malfunctioning shunt part is difficult to identify. To the best of our knowledge, there is no consensus imaging approach for standardizing the evaluation of CSF shunts [8, 19, 20]. Moreover, the importance of 3D-DRIVE in shunt assessment was investigated in only one study [3], and the significance of phase contrast (PC) MR sequence in the evaluation of CSF shunts was discussed in a few papers in the literature [11, 21]. In addition, the value of MRI in the assessment of the abdominal end of the shunt was not thoroughly investigated. Our aim is to study the utility of different MR pulse sequences in evaluating the cranial and abdominal ends of CSF shunts in order to identify the potential cause of shunt failure and its impact on patient management.

Methods

After ethical committee approval, a prospective cohort study was conducted at our institution. The patients included in the study were either referred for routine follow-up or having symptoms suggestive of subacute or chronic shunt malfunction. The latter group included patients with headache, decline in their visual abilities or eye motility, unsteady gait, mood changes, decreased school performance, psychomotor retardation, new onset or increased frequency of seizures, vomiting, abdominal pain or increased abdominal girth, swelling, or CSF leakage along the shunt track. Younger infants could present with increasing occipitofrontal circumference, bulging fontanelle, poor feeding, somnolence, or decreased activity. Patients with rapidly decreasing conscious level, apneic spells, bradycardia, or pupillary alterations were excluded from the study, as these signs indicate brain herniation and require emergent management [22]. As we aimed to assess the abdominal end of the shunt, patients with ventriculoatrial and ventriculopleural shunts were also excluded. Finally, 25 patients were enrolled in the study. An informed consent was provided by the patients or their guardians.

All patients were subjected to history taking and full neurological examination at presentation. After the acquisition of images, patients were followed, and surgical details were documented if they underwent surgery. At surgery, shunts were visually inspected and tested for patency of the proximal and distal catheter ends via reservoir injection and detection of distal runoff, respectively. Patients were further categorized based on the location of the shunt malfunction (as having abnormalities related to the cranial end, abdominal end, or both).

Abdomino-pelvic ultrasound

Abdomino-pelvic ultrasound scan was performed on all patients in the supine position using both linear and convex ultrasound transducers (7.5–11 MHz and 2.5–7.5 MHz, respectively, GE LOGIQ P9 ultrasound machine, USA) by the same radiologist (7 years of experience) who later participated in the MRI imaging analysis. All abdominal quadrants were scanned. The abdominal end of the shunt was traced, and the related fluid was assessed (either free, localized, or absent).

MRI examination

Pediatric patients younger than 5 years of age were sedated prior to the MRI scan using chloral hydrate (100 mg/ml); the dose was calculated according to body weight (100 mg/kg, maximum dose for infants $\leq$1 year 1 gm/dose and for pediatric >1 year 2 gm/dose) according to our Radiology and Anaesthesia departments' guidelines.

All patients were scanned in a supine position by using a 3 T machine (Achieva dStream, Philips medical system, Eindhoven, The Netherlands) using an eight-channel SENSE head coil (SENSE acceleration factor of 16) for brain scan and appropriate Torso coil (SENSE acceleration factor of 32) for the acquisition of abdominal images.

For assessment of the cranial end of the shunt, high-resolution 3D-DRIVE was acquired in the coronal plane. Other conventional brain sequences (diffusion-weighted imaging (DWI), fluid attenuation inversion recovery (FLAIR), T1-WI, T2-WI, and susceptibility-weighted imaging (SWI) in axial planes) were also obtained. ECG-gated quantitative PC sequence was acquired perpendicular to the long axis of the shunt catheter at the suboccipital region distal to its valve, the location where it was settled and unaffected by breath movement. A circular region of interest (ROI) was adjusted over the inner diameter of the shunt in the resultant axial re-phased image by the same radiologist (7 years of experience), and then QF processing software was applied to estimate CSF flow curve and velocity parameters (Fig. 1). For

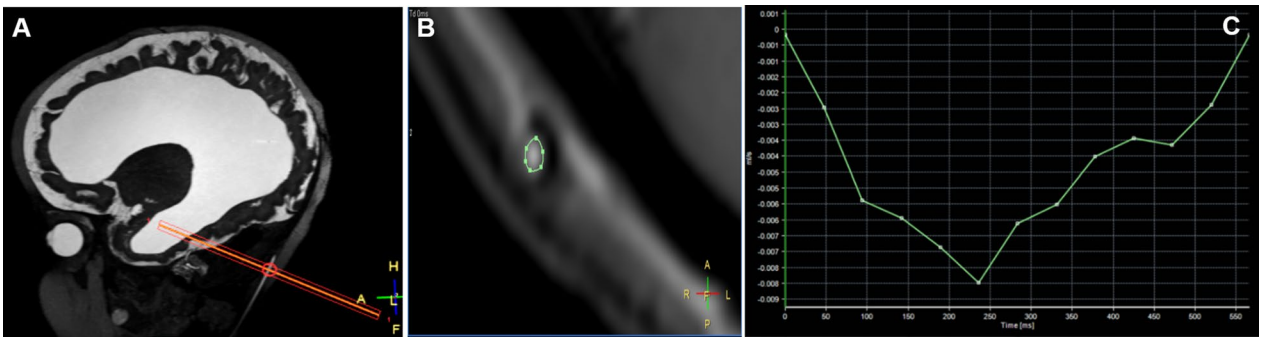

Fig. 1 (**A**, reconstructed 3D-DRIVE in sagittal plane) ECG-gated quantitative PC was acquired perpendicular to the long axis of the shunt catheter at the suboccipital region distal to its valve. **B** A ROI was drawn over the inner diameter of the shunt tube in axial re-phased image. **C** CSF flow curve and velocity parameters were calculated by CSF-QF software

assessment of the abdominal end of the shunt, abdomino-pelvic T2 spectral presaturation with inversion recovery (T2 SPIR) was acquired in axial, coronal, and sagittal planes. (Detailed MRI sequences' parameters are listed in Table 1.)

Image analysis

MRI images were analyzed by two radiologists having 7 and 20 years of experience. The utility of each pulse sequence was assessed according to its ability to precisely locate the cranial portion of the shunt, visualization of its lumen, as well as evaluating the ventricular system, periventricular white matter and the presence of collections or blood products. The shunt reservoir and valve were also assessed regarding the presence of related collection or catheter disconnection. The shunt catheter was considered patent if it had fluid signal within its lumen, whereas the presence of intraluminal low T2 signal intensity could suggest luminal occlusion [3]. Abdominal sequences were assessed according to their ability to localize the abdominal end of the shunt and assess the related fluid collections.

Statistical analysis

In patients with multiple inserted shunts, the findings of the most recently inserted shunt were used in statistical analysis. The importance of each sequence was determined by its ability to detect additional information that other sequences did not provide, or whether it provided clinically valuable data when compared to other sequences.

Table 1 Detailed MRI sequences' parameters

	TR/TE (ms)	FOV (mm)	Matrix	NEX	Flip angle	Section thickness (mm)	Gap (mm)	Duration (in min)
Brain (localizer)	15/5.3	250 × 250	256 × 126	1	20 °	3	10	0.3
DWI	2867/76	230 × 200	124 × 98	2	90°	5	1	1.2 ± 0.2
T1-WI	713/2.3	230 × 200	224 × 179	1	80°	5	1	1.4 ± 0.4
T2-WI	7440/110	230 × 200	224 × 179	1	90°	5	1	1.4 ± 0.6
FLAIR	1100/130	230 × 200	208 × 132	2	90°	5	1	2.7 ± 0.4
SWI	31/7.2	230 × 200	333 × 332	1	17 °	2	1	3.2 ± 0.5
3D-DRIVE	2000/240	220 × 190	476 × 380	1	90°	1	-0.5	8.8 ± 1.2
QF	12/7.5	105 × 105	180 × 126	1	15 °	4	0	2.8 ± 0.6
Abdomino-pelvic localizer	8/2.3	450 × 450	256 × 128	1	15 °	5	10	0.25
Abdomino-pelvic T2 SPIR	1100/70	300 × 260	188 × 166	1	90 °	4	1	1 ± 0.6 (axial) 0.7 ± 0.4 (coronal) 0.9 ± 0.5 (sagittal)

DWI diffusion-weighted imaging, T1-WI T1-weighted image, T2-WI T2-weighted image, FLAIR fluid attenuation inversion recovery, SWI susceptibility-weighted imaging, 3D-DRIVE three-dimensional driven equilibrium, QF quantitative flow, T2 SPIR T2 spectral presaturation with inversion recovery. TRrepetition time, TE echo time, NEX number of excitations

FOV field of view and Matrix (vary according to patients' head and abdominal size)

The relation between ventricular catheter location and its proximity to the surrounding structures with its luminal patency was studied and statistically tested using the Fisher's exact test.

The catheter luminal flow distal to the valve was quantitatively analyzed on the quantitative PC sequence. The estimated results (flux and mean velocity values) for patent shunts were statistically compared to those with complications. Asymptomatic patients and patients with suspected shunt malfunction were compared regarding the presence of dilated ventricles and abnormal periventricular white matter signal intensity. Patients who underwent surgery and those who underwent conservative management were compared regarding the presence of shunt-related abnormalities as well with the estimation of the positive and negative likelihood ratios.

Results

Twenty-five patients (18 males, 7 females, median age 2.5 years, IQR 0.75–15) were enrolled in the study. There were eight asymptomatic patients who were referred for routine follow-up, and 17 patients (having 21 shunts) who experienced symptoms suggestive of shunt malfunction. Three patients had more than one inserted shunt. Finally, there were 28 VP shunts and single ventriculogallbladder (VGB) shunt; all had first-generation type valves (fixed differential pressure valves with no related motion or metallic artifacts). An average of 15 min was required for the sedation of children under the age of 5 prior to the MRI scan.

3D-DRIVE (in coronal plane supplemented by axial, sagittal, and various obliquities reformations) was able to precisely assess the cranial portion of all evaluated shunts regarding their location, integrity, luminal patency, and periventricular white matter signal alteration (Fig. 2). In addition, ventricular system and extra-axial spaces anatomical details were well demonstrated in all patients. Although axial FLAIR and T2-WI were able to assess the ventricular size and periventricular white matter signal intensity, they failed to precisely demonstrate the catheter lumen. In addition, ventricular loculations were demonstrated similarly on T2-WI and 3D-DRIVE in four patients; however, the fine internal ventricular septae related to the shunt were only perceived in 3D-DRIVE in three patients ($p < 0.001$) (Fig. 3).

Extra-axial hematoma was detected in four patients. Determination of signal intensity on T1-WI, and T2-WI, or 3D-DRIVE was valuable in the determination of the age of the subdural collection (Fig. 4). Three patients had a subacute hematoma and one had a chronic collection. Variable diffusion restriction was seen only in two patients. SWI demonstrated old hemosiderin foci (in 14 patients). Both DWI and SWI were found to have less considerable clinical value in terms of patients' management.

Abdomino-pelvic T2 SPIR was able to evaluate the abdominal end of the shunt in all patients and to detect related complications (either loculated intraperitoneal collection (CSF pseudocyst), extraperitoneal migration, CSF ascites, or absent intraperitoneal fluid). However, only two planes could be sufficient for three-dimensional assessment for cases with the loculated collection. The findings of abdomino-pelvic MRI scan were in excellent agreement with ultrasound findings (Cohen's Kappa 0.9). However, compared to ultrasound, MRI was unable to detect a small gallbladder wall defect in the only patient with a VGB shunt who developed CSF pseudocyst (Fig. 5).

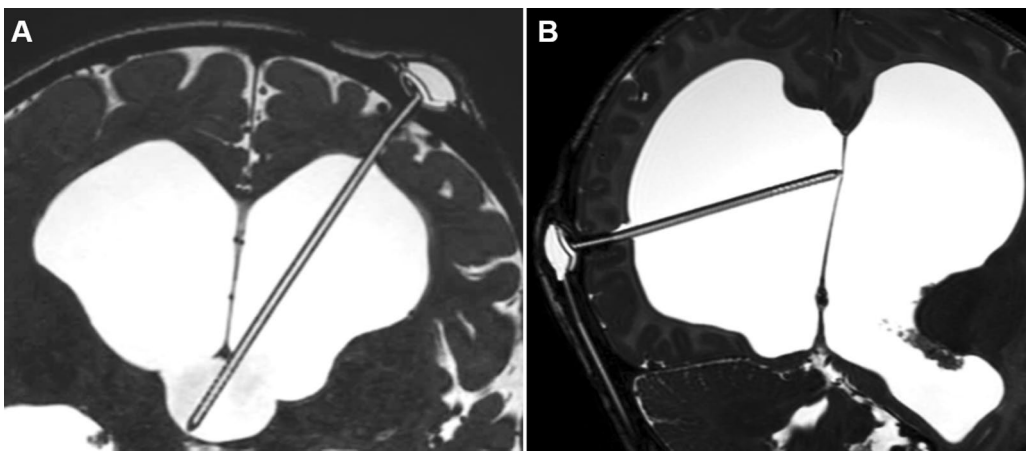

Fig. 2 Reconstructed 3D-DRIVE in axial oblique plane (**A**) and coronal oblique plane (**B**) demonstrates luminal CSF signal throughout a patent cranial portion of shunt

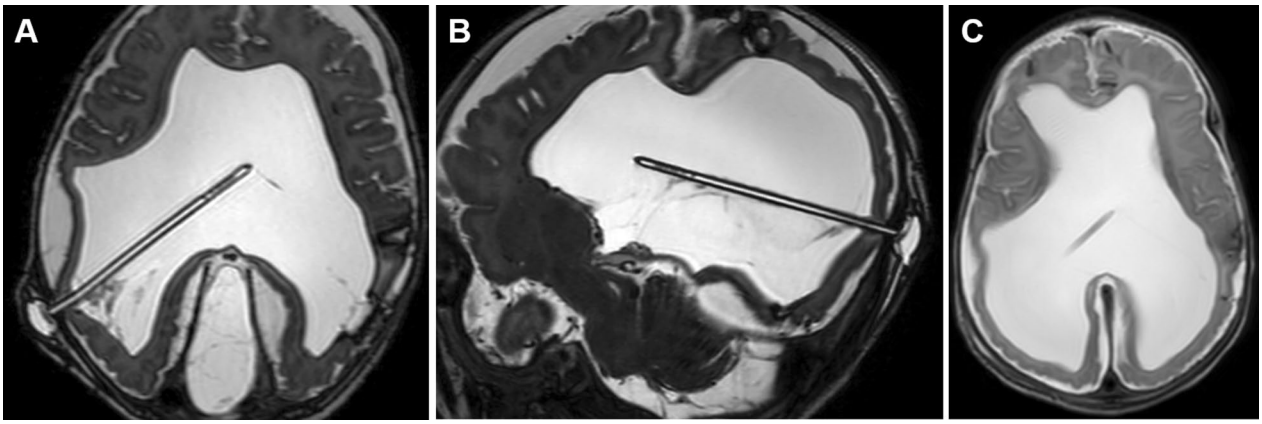

Fig. 3 A 2-month-old boy presented with fever and poor feeding. **A**, **B** Reconstructed 3D-DRIVE in axial and sagittal oblique planes, respectively, shows multiple fine ventricular septae surrounding proximal catheter that shows intraluminal faint low signal, which may represent intraluminal extension of these septae along with luminal debris. **C** Axial T2-WI for the same patient does not show any intraventricular septae or shunt catheter lumen

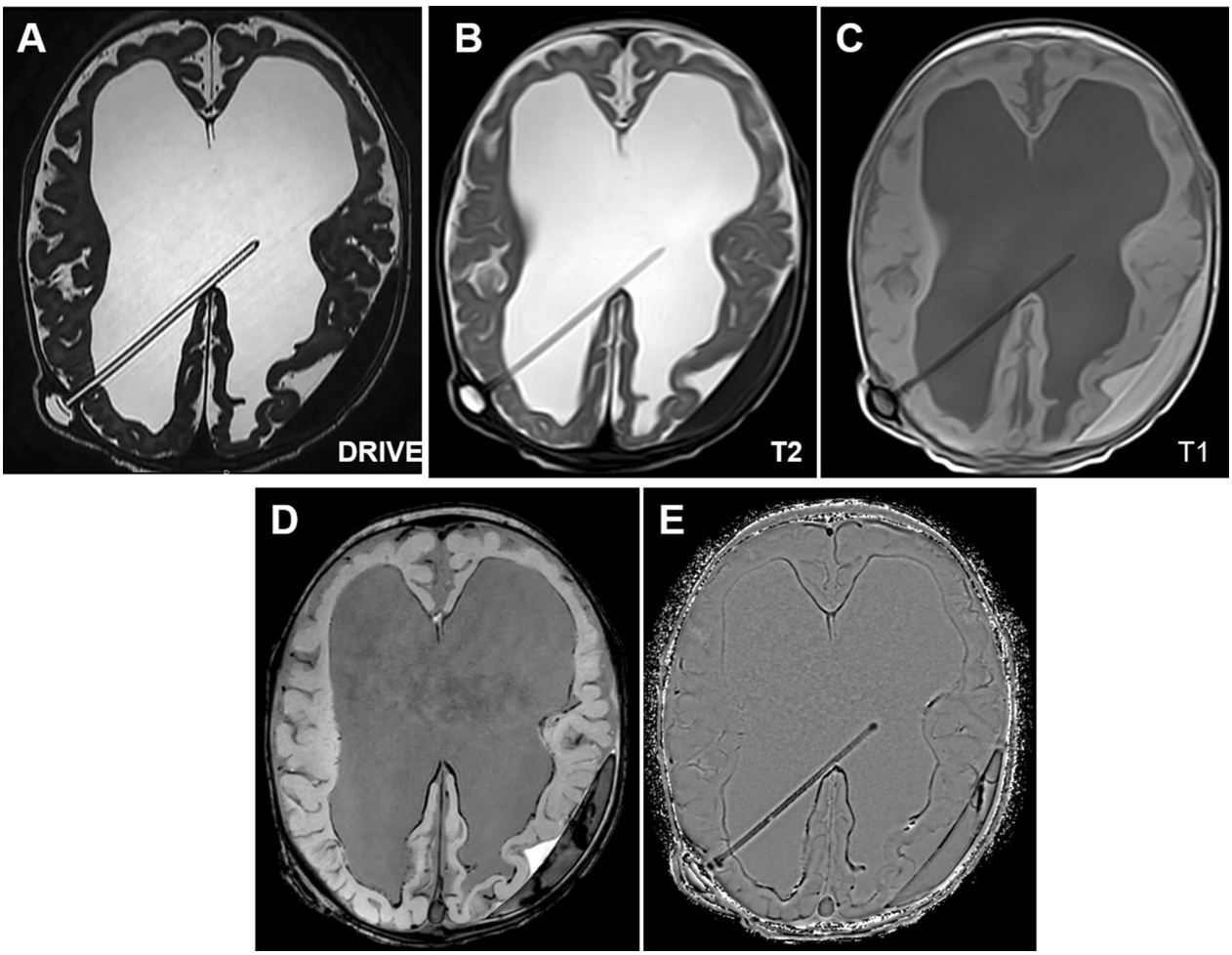

Fig. 4 A 7-month-old boy was referred for routine follow-up. Left parieto-occipital early subacute subdural hematoma that displays similar hypointense signal in both 3D-DRIVE and T2-WI and hyperintense signal in T1-WI, related foci of blooming artifact in SWI (**D**, **E** magnitude and phase images, respectively) with no related diffusion restriction (not shown). The proximal catheter and reservoir of the shunt are patent, both demonstrating luminal CSF signal (seen in **A**)

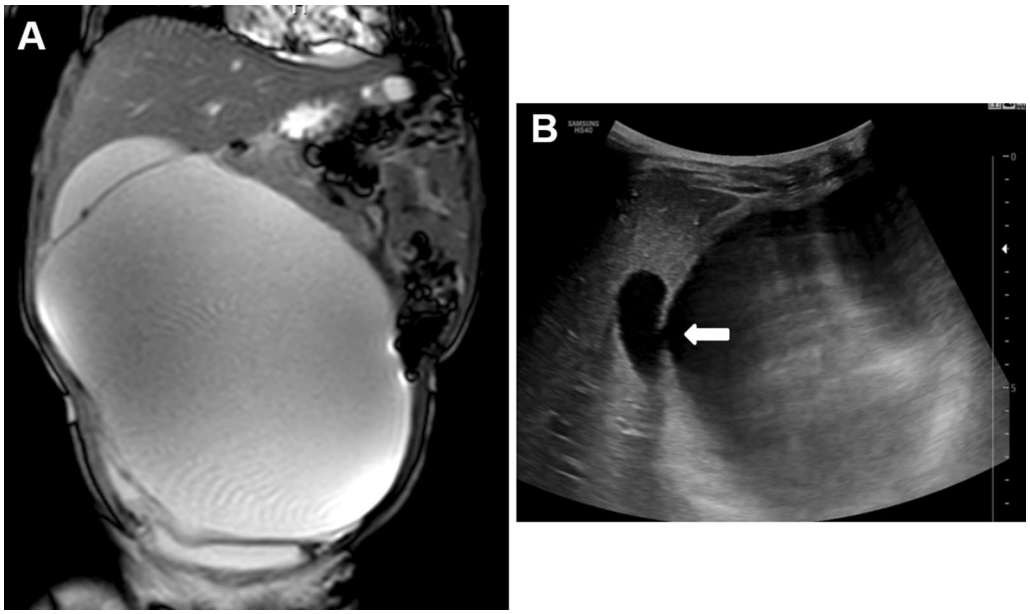

Fig. 5 A 2-year-old boy with ventriculo-gallbladder shunt presented with increasing abdominal girth. **A** Coronal abdomino-pelvic T2 SPIR and **B** corresponding ultrasound show a large abdomino-pelvic loculated fluid (CSF pseudocyst) with gallbladder mural defect (arrow) demonstrated in ultrasound image

The luminal patency of the shunt proximal catheter was found to be correlated with the exact location of its terminal portion and the nature of the surrounding structures (*p*: 0.002). An altered intraluminal signal was demonstrated in 8 shunts; all were located either in close proximity to the choroid plexus, or surrounded by intraventricular septae. And, of the seventeen totally patent proximal catheters, eleven were found to be freely located within the lateral ventricle away from the choroid plexus.

Quantitative PC sequence was evaluated in only 19 shunts: patent shunts (8), cranial end complications (7), and abdominal end complications (5), the remaining shunts were excluded from the analysis due to motion artifact. The flux and mean velocity of patent shunts were found to be 0.03 ml/s and 0.3 cm/s, respectively. All shunts with cranial end complications had weak flux and lower mean velocity values (0.008 ml/s and 0.16 cm/sec, respectively), except for one patient who had a CSF collection surrounding shunt reservoir, she had accelerated flow (flux: 0.1 ml/sec, mean velocity: 2.2 cm/sec). Shunts with abdominal end complications had relatively higher flux and mean velocity values (0.057 ml/sec and 1.1 cm/sec, respectively). However, there was no statistically significant difference regarding flux and velocity values between patients with complicated shunts and those with patent shunts (p: 0.5 and 0.3, respectively).

Detailed MRI findings for patients are summarized in Tables 2 and 3. Among asymptomatic patients, total luminal patency of the cranial portions of the shunts was demonstrated in all but one patient. Abdominal sequences revealed minimal free intraperitoneal fluid in all but one patient (Patient 8; Table 2); his MRI showed appreciable amount of free intraperitoneal fluid (CSF ascites) (Fig. 6).

Despite clinical suspicion of shunt malfunction, total luminal patency of the cranial portions of the shunts was demonstrated in four shunts, with related minimal free intraperitoneal fluid around their abdominal ends (Patients 1–4; Table 3). However, shunt malfunction attributed to cranial end complications was demonstrated in eight symptomatic patients (Patients 5–12; Table 3) in the form of intraluminal faint or dark signal signifying luminal occlusion (Fig. 3, 7), catheter disconnection from the reservoir/valve (Fig. 8), extraventricular course of the proximal catheter (Fig. 9), isolated fluid collection surrounding shunt reservoir (Fig. 10), or slit ventricle with possible overshunting. Shunt malfunction attributed to abdominal end complications was demonstrated in three patients (Patients 15–17; Table 3). Two patients were found to have loculated intraperitoneal fluid collections (CSF pseudocysts) (Fig. 5), while the abdominal scans of the third patient did not show the expected minimal free intraperitoneal fluid. Combined cranial and abdominal end complications were demonstrated in two other patients (Patients 13, 14; Table 3).

Among patients having cranial end-related complications (11 patients, two of them had additional

Table 2 Clinical and MRI findings of asymptomatic patients

Patient	Age	Indications for shunting	Location of the shunt complication	Management	Cranial end	Abdominal end	Ventricular dilatation	White matter abnormal signal	Phase contrast (Flux/mean velocity) (ml/sec and cm/sec)
1	2.5 Y	Congenital hydrocephalus	No shunt-related abnormality	Conservative	Patent	Minimal free fluid	Dilated	Absent	0.01/0.04
2	11 M	Congenital hydrocephalus	No shunt-related abnormality	Conservative	Patent	Minimal free fluid	Dilated	Absent	0.01/0.12
3	4 Y	Congenital hydrocephalus	No shunt-related abnormality	Conservative	Patent	Minimal free fluid	Dilated	Absent	0.05/0.46
4 **(Fig. 4)**	7 M	Congenital hydrocephalus	No shunt-related abnormality	Conservative	Patent	Minimal free fluid	Dilated	Absent	0.01/0.28
5	8 M	post-meningoencephalitis	No shunt-related abnormality	Conservative	Patent	Minimal free fluid	Dilated with internal loculations	Present	0.03/0.09
6	11.5 M	post-meningoencephalitis	No shunt-related abnormality	Conservative	Patent	Minimal free fluid	Dilated with internal loculations	Present	0.09/0.63
7	9 Y	Operated posterior fossa tumour	Cranial end	Conservative	Intraluminal low signal	Minimal free fluid	Not dilated	Absent	0.004/0.1
8[#] (Fig. 6)	6 M	Congenital hydrocephalus	Abdominal end	Insertion of VA shunt	Patent	CSF ascites	Dilated	Absent	0.02/0.39

[#] on follow-up, this patient experienced increasing occipitofrontal circumference and he underwent an alternative CSF diversion (ventriculoatrial, VA shunt insertion)

abdominal end complications), eight underwent surgery. The remaining three patients underwent conservative management despite the apparent shunt complication (Patient 7; Table 2 and Patients 9, 12; Table 3); two of them could be independent of the occluded shunt, as one had no obstructing lesions at the time of the MRI scan and the other had metastatic brain lesions on treatment. The third patient had overshunting. However, among the ten patients with no shunt-related abnormalities, only one patient (Patient 1; Table 3) underwent surgery (as additional shunt was inserted in an entrapped CSF pocket) ($p < 0.001$), positive likelihood and negative likelihood ratios = 7.27, 0.3, respectively, sensitivity = 0.7, specificity = 0.9). All patients with abdominal end-related complications (4 patients) underwent shunt revision ($p < 0.001$). There is no significant difference between patients who underwent surgery and those with conservative management, or symptomatic and asymptomatic patients in terms of the prevalence of ventricular dilatation or white matter signal abnormality (p: 0.6 and 0.3, respectively).

Discussion

The diagnosis of CFS shunt malfunction could be clinically challenging [2, 20]. Moreover, there is no standardized diagnostic imaging protocol to evaluate CSF shunts [8, 20]. We aimed to demonstrate the value of different MR pulse sequences in evaluating both the cranial and abdominal ends of CSF shunts in order to guide patient management. Guided by the patients' clinical scenarios and presenting symptoms, each institution determines its imaging protocol in accordance with its available resources [15].

Fast MRI brain sequences (single-shot T2 sequences, e.g., HASTE) could be adopted in the setting of acute patient presentation [13–15]. Alternatively, low-dose pediatric unenhanced CT protocols could be used if MRI is not available [15]. CT and fast MRI sequences depend on the assessment of the ventricular size and configuration, localization of the shunt, and detection of periventricular white matter signal alteration [15]. However, shunt may fail without ventricular dilatation [23, 24] and, white matter signal alteration could be not only secondary to transependymal CSF permeation but also due to

Table 3 Clinical and MRI findings of symptomatic patients

Patient	Age	Indications forshunting	Location of the shunt complication	Management	Cranial end	Abdominal end	Ventricular dilatation	White matter abnormal signal	Phase contrast (flux/mean velocity)(ml/sec and cm/sec)
1	4.5 Y	Post-meningoencephalitis	No shunt-related abnormality	Insertion of an additional shunt in the entrapped CSF pocket	Patent	Minimal free fluid	Dilated with internal loculations and entrapped CSF pockets	Present	0.01/0.5
2	1.25 Y	Post-meningoencephalitis	No shunt-related abnormality	Conservative	Patent	Minimal free fluid	Dilated	Absent	
3	7 M	Post-meningoencephalitis	No shunt-related abnormality	Conservative	Patent	Minimal free fluid	Dilated	Absent	0.01/0.24
4 (had three shunts) (Fig. 8)	27 Y	Post-meningoencephalitis	The recent shunt had no related abnormality	Conservative	Patent* Patent with proximal catheter disconnection Intraluminal faint low signal with distal catheter disconnection	Minimal free fluid	Dilated	Absent	
5	27 Y	Post-meningoencephalitis	Cranial end	Shunt revision	Intraluminal low signal with distal catheter disconnection	Minimal free fluid	Dilated	Absent	0.01/0.01
6 (Fig. 3)	2 M	Congenital hydrocephalus	Cranial end	Shunt revision	Intraluminal low signal	Minimal free fluid	Dilated with fine internal septae surrounding the shunt	Absent	0.01/0.2
7 (Fig. 7 A)	15 Y	Idiopathic communicating hydrocephalus	Cranial end	Shunt revision	Intraluminal dark signal, was close to the choroid plexus	Minimal free fluid	Dilated	Absent	0.005/0.25
8 (Fig. 7 B)	24 Y	post-meningoencephalitis	Cranial end	Insertion of an additional shunt	Intraluminal dark signal	Minimal free fluid	Dilated with fine internal septae surrounding the shunt	Present	
9	65 Y	Multiple brain metastasis	Cranial end	Conservative	Intraluminal dark signal, was close to the choroid plexus	Minimal free fluid	Not dilated	Present	0.01/0.16
10 (Fig. 9 A)	9 M	post-meningoencephalitis	Cranial end	Shunt revision	Extraventricular	Minimal free fluid	Dilated with internal loculations	Absent	
11 (Fig. 10)	9 M	Congenital hydrocephalus	Cranial end	Shunt revision	Patent with fluid collection surrounding the reservoir	Minimal free fluid	Dilated with ventricular diverticulum	Absent	0.1/2.2

Table 3 (continued)

Patient	Age	Indications forshunting	Location of the shunt complication	Management	Cranial end	Abdominal end	Ventricular dilatation	White matter abnormal signal	Phase contrast (flux/mean velocity)(ml/sec and cm/sec)
12	7 Y	Congenital hydrocephalus	Cranial end	Conservative	Patent	Minimal free fluid	Slit-like ventricles suggesting overshunting	Absent	0.01/0.23
13[#] (had two shunt) (Fig. 9 B)	36 Y	Posterior fossa neoplasm	Cranial and abdominal end	Shunt revision	[*]Intraluminal low signal, was close to the choroid plexus	Extraperitoneal migration	Not dilated	Present	
					Intraluminal dark signal, was embedded within septum pellucidum	No peritoneal fluid			
14	3 Y	Congenital hydrocephalus	Cranial and abdominal end	Shunt revision	Intraluminal low signal, was embedded within choroid plexus	CSF pseudocyst complicated with abdominal wall sinus	Not dilated	Absent	
15	1.25 Y	post-meningoencephalitis	Abdominal end	Shunt revision	Patent	CSF pseudocyst	Dilated	Present	0.02/0.38
16[##] (Fig. 5)	2 Y	Congenital hydrocephalus	Abdominal end	Shunt revision	Patent	CSF pseudocyst	Dilated with fine internal septae	Present	0.08/2.2
17 (had two shunts)**	41 Y	Congenital hydrocephalus	Abdominal end	Shunt revision and omental plugging confirmed at surgery	Patent	No peritoneal fluid	Dilated	Present	0.1/1.7

*Recently inserted shunt

**Both shunts had the same findings

#Obese patient with body mass index 44.4

##Patient with ventriculo-gallbladder shunt

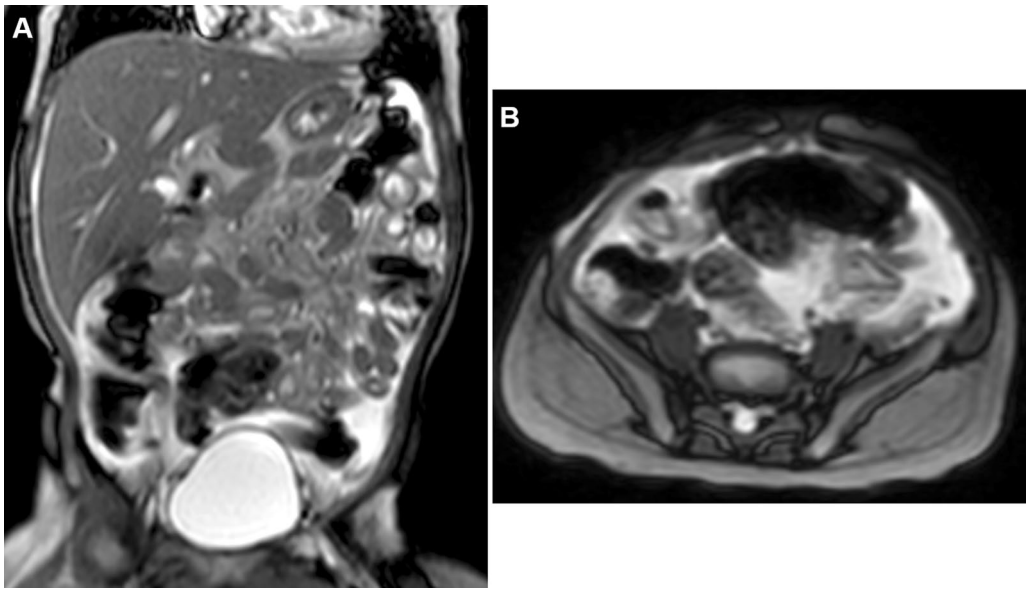

Fig. 6 A 6-month-old boy was referred for routine follow-up. **A**, **B** Abdomino-pelvic T2 SPIR in coronal and axial planes, respectively, shows large volume of free ascites (CSF ascites). The cranial portion of this shunt is patent (not shown). This patient experienced increasing occipitofrontal circumference during regular follow-up visits (1.5 months after imaging), and he underwent an alternative CSF diversion (VA shunt insertion)

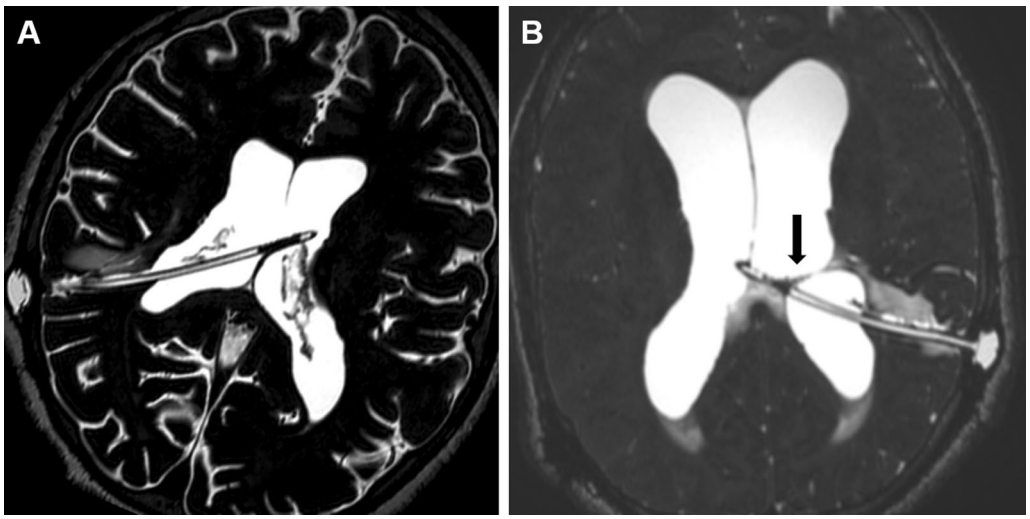

Fig. 7 Reconstructed 3D-DRIVE in axial oblique planes. **A** A 15-year-old male patient presented with unsteady gait and convergent squint, **B** A 24-year-old male patient presented with headache and attacks of vomiting. Both show proximal catheter intraluminal dark signal occluding segment where side holes are located, closely adjacent to left lateral ventricular choroid plexus (could suggest choroid plexus ingrowth). In addition to transependymal permeation and adhesion between proximal catheter terminal part and related ventricular ependymal lining (arrow) in (**B**)

defective myelination [18]. Moreover, our results did not reveal any statistically significant difference between symptomatic and asymptomatic patients regarding the presence of ventricular dilatation or periventricular white matter signal alteration. This could decrease the reliability of both signs, and hence CT and rapid MRI sequences, in the diagnosis of shunt malfunction.

The most frequent cause of shunt malfunction is shunt catheter blockage, which may be caused by debris or blood clots early postoperatively, or secondary to choroid plexus ingrowth in long-term shunts [12, 25]. Additionally, intraventricular adhesions/septae, which can develop as a complication of neonatal meningitis or intraventricular hemorrhage, can surround and embed

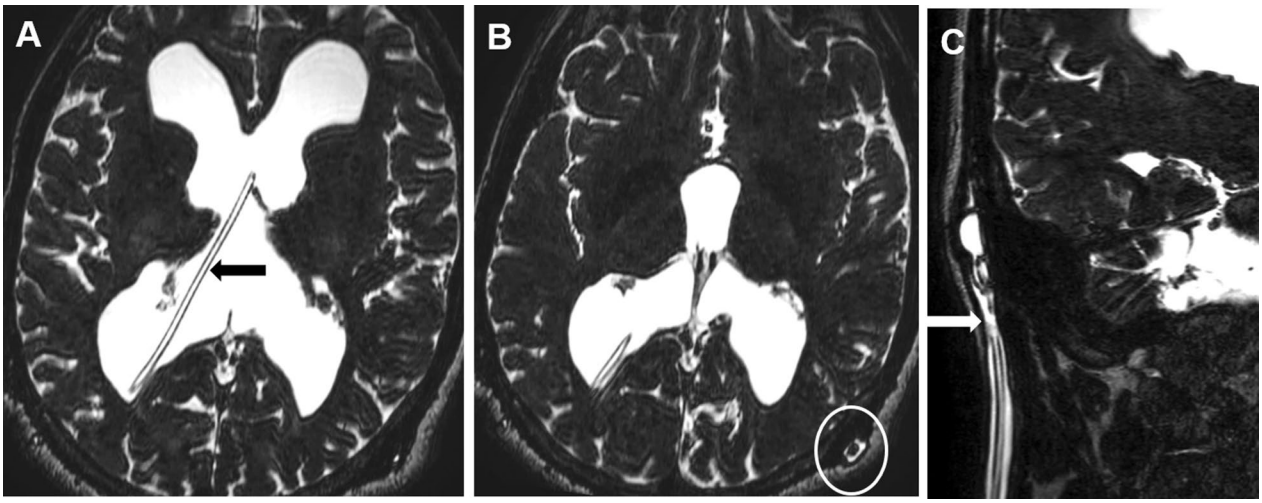

Fig. 8 A 27-year-old male patient presented with headache and blurring of vision. Reconstructed 3D-DRIVE for the same patient who had 3 shunts, (**A**, **B**) in axial plane, showing collapsed reservoir (circle) with separated its proximal catheter (black arrow), (**C**) in coronal oblique, showing separated distal catheter from its valve with related fluid (white arrow); he had another right frontal shunt (non-complicated, not shown)

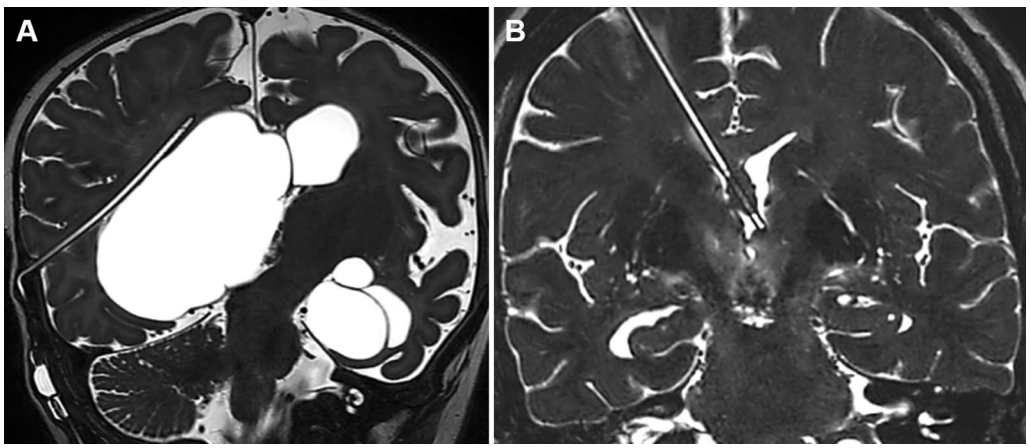

Fig. 9 Reconstructed 3D-DRIVE in coronal oblique planes, **A** A 9-month-old asymptomatic boy, yet the clinical examination of his shunt showed poor filling of the reservoir, shows extraventricular migration of the proximal catheter. **B** A 36-year-old female patient presented with fluctuating conscious level, shows embedded proximal catheter (terminal 2 cm) within septum pellucidum and shows intraluminal dark signal

ventricular catheters resulting in shunt malfunction [26]. Both CT and fast MRI sequences have low sensitivity in the assessment of the shunt catheter lumen. Our study revealed that PHILIPS-developed 3D-DRIVE sequence had significant advantages over other sequences. Similar sequences were developed by GE and Siemens manufacturers (Fat Imaging Employing Steady-State Acquisition FIESTA, Constructive Interference In Steady State CISS, respectively). 3D-DRIVE can clearly demonstrate the ventricular catheter lumen as previously documented [3]; in addition, fine intraventricular adhesions/septae and its relation to the catheter were adequately visualized [3, 17]. We have found that the location of the proximal catheters' terminal part and its relation to the surrounding structures, especially choroid plexus, significantly affect the proximal catheter patency and could indicate the cause of obstruction as previously documented [27, 28].

T2-WI and FLAIR sequences did not add additional diagnostic information other than those found in the 3D-DRIVE sequence. In addition, they failed to demonstrate the shunt catheter lumen and the fine intraventricular septations related to the shunt. T1-WI was found to be of value in aging determination of the hematomas in combination with T2-based DRIVE [29]. DWI and SWI could be considered as non-essential sequences in

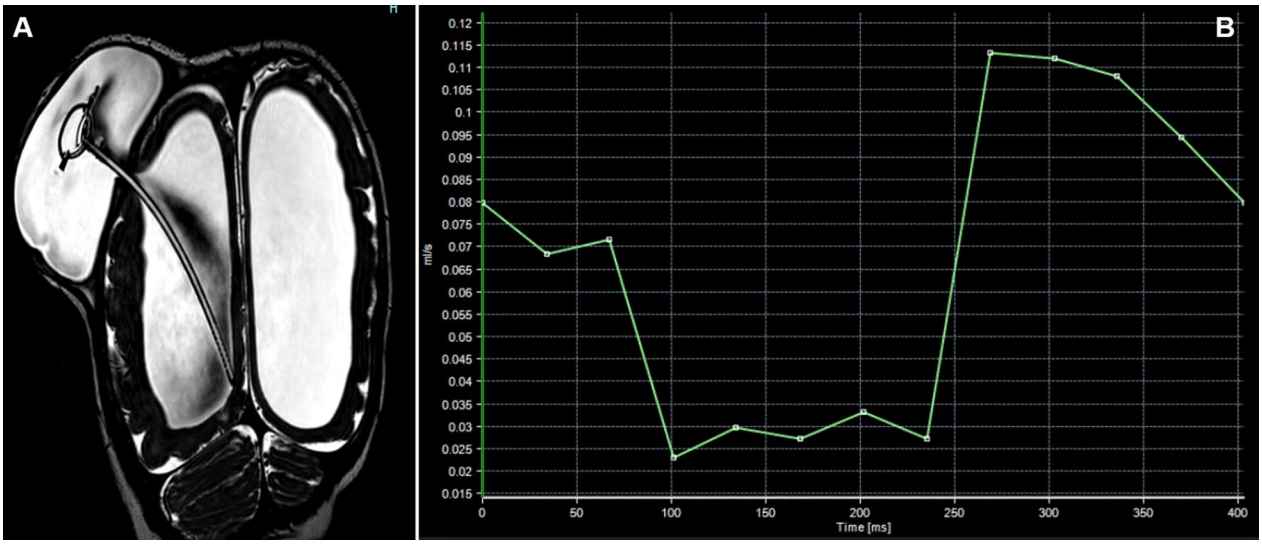

Fig. 10 A 9-month-old girl presented with scalp swelling. **A** Reconstructed 3D-DRIVE in coronal oblique plane shows fluid collection surrounding shunt reservoir near skull burr hole; the proximal catheter and reservoir are seen patent with no evidence of disconnection. Turbulent CSF flow-related artifact is noted within the ventricular system and fluid collection as well (appreciated in FLAIR sequence, not shown). **B** CSF flow curve shows high flow rate values (flux: 0.1 ml/sec)

the setting of suspected shunt malfunction, despite their known role in the standard neuroimaging protocol.

It was reported that enhanced sequences following intravenous contrast administration could be added to distinguish choroid plexus ingrowth from other causes of luminal occlusion, as fatal intraventricular hemorrhage may occur during attempts to remove these retained ventricular catheters [3, 30, 31]. Nevertheless, contrast-enhanced sequences were not added to our protocol. Contrast injection is time-consuming. In addition, it might be contraindicated in some circumstances or for some individuals with renal impairment. Moreover, any ventricular catheters that revealed luminal blockage should be handled properly, taking the risk of hemorrhage into account [26, 31]. However, when shunt-related infections are clinically suspected, contrast could be used to demonstrate abnormal enhancement pattern of leptomeningeal and ventricular ependymal lining that are typical with meningitis and ventriculitis, respectively [12, 32].

Shunt catheter fractures or disconnection accounts for 4.5–13.6% of shunt failure [33]. Catheter disconnection usually occurs in the neck as it is the most mobile part of the body [33, 34]. DRIVE sequence with its three-dimensional capabilities was able to demonstrate catheter disconnection either proximal or distal catheter from reservoir or valve, respectively. Catheter fractures along the subcutaneous tunneled distal catheter could be diagnosed by radiographic shunt series [35, 36]. However, the diagnostic yield and sensitivity of the radiographic shunt series are very low; it can detect the cause of malfunction in less than 10% of pediatric patients and even fewer adult shunts [3, 35, 36]. It was documented that patients with suspected shunt malfunction should proceed with more reliable images, and the use of shunt series should be restricted to patients with clinical suspicion of mechanical cause of shunt malfunction, and non-diagnostic other tests [35, 36]. None of our patients required radiographic shunt series for their diagnosis.

Few reports have described the role of cross-sectional imaging in identifying shunt malfunction attributed to abdominal end complications [2, 12, 32, 37, 38]. In our dataset, MRI showed excellent agreement with ultrasound and operative findings, making MRI a good one-stop destination for assessment of patients with suspected shunt malfunction. The presence of minimal free fluid within the peritoneal cavity could be considered an indicator of healthy peritoneal membrane [39]. The presence of CSF collections or absence of peritoneal fluid despite patent cranial end are signs of abdominal end-related complications [2, 40]. The latter finding could be explained by omental plugging within the side holes of the shunt. Tiny omental projections insinuate through the catheter side holes causing luminal blockage. It has an estimated incidence between 7 and 18% [11, 40]. On the contrary, sterile CSF ascites is considered a rare abdominal complication of the VP shunt that can occur secondary to defective peritoneal CSF absorptive capacity or secondary to choroid plexus CSF overproduction, and in this instance, it is necessary to use an alternative

CSF diverting technique (such as a ventriculoatrial or VGB approach) or choroid plexus cauterization, respectively [41, 42]. Other causes of abdominal end complications include extraperitoneal catheter migration that was documented in obese patients with raised intraabdominal pressure that can impair CSF drainage or lead to catheter migration [2, 43–45].

Failure of adequate control of hydrocephalus implies shunt failure which is clinically indicated by shunt removal, revision, or replacement [33]. Shunt malfunction was confirmed at surgery in all operated patients. Apart from three patients, all patients with cranial and/or abdominal end complications underwent surgery (either shunt revision or an additional shunt was inserted, which confirms shunt failure). All apart from one patient with no catheter-related abnormality underwent conservative management. MRI results were found to have a high diagnostic performance for the assessment of patients with suspected shunt malfunction.

Quantitative PC assessment of patent shunts showed sluggish flux and low mean velocity values, as the patients were scanned while supine, where the hydrostatic pressure difference between the abdominal cavity and the ventricular system is almost zero. This could be explained by the normalized intracranial pressure and subsequent lack of driving force for CSF flow inside the shunt system [46].

Prior studies revealed low-velocity values in malfunctioned shunts, irrespective of the site and type of shunt malfunction [11, 21]. However, we have found that quantitative PC assessment varied depending on the location and type of shunt-related complication. Shunts with proximal catheter intraluminal signal alteration and those with overshunting were found to have sluggish flux and lower mean velocity values. The perceived sluggish flow in occluded shunts could be explained by partial rather than total occlusion of shunt side holes. It was documented that, CSF can flow within a normal range of flow rates even while the ICP is dangerously elevated due to the buildup of CSF and the ensuing increase in ICP [46–48]. In the setting of shunt fracture or disconnection, CSF flow could be dependent on the presence of fibrous tract at the site of the shunt discontinuity [48]. On the contrary, the patent shunt with CSF collection surrounding the reservoir and those with abdominal end-related complications were found to have relatively higher flux and mean velocity values than those with patent shunts. Similarly, brisk CSF flow was found during CSF shunt scintigraphy, which could be indicative of valve malfunction or complications in the drainage compartment or distal catheter. [48]. Although PC assessment did not show statistically significant differences between patients with complicated and patent shunts, the analyzed findings could give insights into CSF dynamics through CSF shunts in patients with different causes of shunt malfunction.

The limitations of our study included a relatively small sample size and a small number of asymptomatic patients with patent shunts. Different commercial shunt types were not taken into consideration. Also, this detailed MRI protocol for shunt assessment could be unsuitable for patients with signs of acute shunt malfunction and possible brainstem herniation in whom timely management is of utmost importance. However, it was found to be clinically relevant in a substantial number of symptomatic patients having subacute or chronic symptoms.

Conclusions

MRI could be a one-stop destination for CSF shunt assessment in patients with suspected non-acute shunt malfunction; 3D-DRIVE and T1-WI of the brain, together with T2 SPIR of the abdomen and pelvis, were found to be essential sequences for evaluation of the cranial and abdominal ends of the CSF shunts, respectively. These sequences were found to have clinical relevance in terms of accurately locating the exact site and possible cause of shunt-related complications.

Abbreviations

MRI	Magnetic resonance imaging
CSF	Cerebrospinal fluid
CT	Computerized tomography
TSE	Turbo spin echo
3D-DRIVE	Three-dimensional driven equilibrium
QF	Quantitative flow
PC	Phase contrast
DWI	Diffusion-weighted imaging
FLAIR	Fluid attenuation inversion recovery
T1-WI	T1-weighted image
T2-WI	T2-weighted image
SWI	Susceptibility-weighted imaging
T2 SPIR	T2 spectral presaturation with inversion recovery
ICP	Intracranial pressure

Acknowledgements

We sincerely appreciate the contributions of Mr. Ashraf Saber, Mr. Ahmed Elsayed, Mr. Mostafa ElKadi, Mr. Ahmed Mahfouz, Mr. Walid Mohamed, and Miss Hadeer Ahmed (MR technicians), as well as Mr. Ahmed Sobhy and Mrs. Heba Farouk for their administrative assistance.

Author contributions

All authors contributed to the study conception and design. Material preparation, data collection, and analysis were performed by EAH, SAM, and AMMA. The first draft of the manuscript was written by EAH. All authors read and approved the final manuscript.

Funding

No funding was obtained for this study.

Availability of data and materials

The datasets used and/or analyzed during the current study are available from the corresponding author upon reasonable request.

Declarations

Ethics approval and consent to participate

The study was approved by the ethical committee of Faculty of Medicine, Ain-Shams University (FMASU REC) under Fedral wide assurance No. FWA00017585 (FMASU MD 263/2020). An informed consent for participation was given by the patients, their parents, or legal guardians.

Consent for publication

Identifying information about participants (patients' identity) did not appear in any part of the manuscript; therefore, consent for publication was not required.

Competing interests

The authors declare that they have no conflict of interest.

Received: 24 January 2023 Accepted: 11 February 2023
Published online: 03 March 2023

References

1. Boyle TP, Nigrovic LE (2015) Radiographic evaluation of pediatric cerebrospinal fluid shunt malfunction in the emergency setting. Pediatr Emerg Care 31:435–440. https://doi.org/10.1097/PEC.0000000000000462
2. Bolster F, Fardanesh R, Morgan T et al (2016) Cross-sectional imaging of thoracic and abdominal complications of cerebrospinal fluid shunt catheters. Emerg Radiol 23:117–125. https://doi.org/10.1007/s10140-015-1368-8
3. Blitz AM, Huynh PP, Bonham LW et al (2020) High resolution MRI for evaluation of ventriculostomy tubes: assessment of positioning and proximal patency. AJNR 63:41–57. https://doi.org/10.3174/ajnr.A6320
4. Kahle KT, Kulkarni AV, Limbrick DD Jr et al (2016) Hydrocephalus in children. Lancet 387:788–799. https://doi.org/10.1016/S0140-6736(15)60694-8
5. Krishnan P, Raybaud C, Palasamudram S et al (2019) Neuroimaging in pediatric hydrocephalus. Indian J Pediatr 86:952–960. https://doi.org/10.1007/s12098-019-02962-z
6. Patel SK, Tari R, Mangano FT (2021) Pediatric hydrocephalus and the primary care provider. Pediatr Clin N Am 68:793–809. https://doi.org/10.1016/j.pcl.2021.04.006
7. Khan AA, Jabbar A, Banerjee A et al (2007) Cerebrospinal shunt malfunction: recognition and emergency management. Br J Hosp Med 68:651–655. https://doi.org/10.12968/hmed.2007.68.12.651
8. Broggi M, Zattra CM, Schiariti M et al (2020) Diagnosis of ventriculoperitoneal shunt malfunction: a practical algorithm. World Neurosurg 137:e479–e486. https://doi.org/10.1016/j.wneu.2020.02.003
9. Lehnert BE, Rahbar H, Relyea-Chew A et al (2011) Detection of ventricular shunt malfunction in the ED: relative utility of radiography, CT, and nuclear imaging. Emerg Radiol 18:299–305. https://doi.org/10.1007/s10140-011-0955-6
10. Sellin JN, Cherian J, Barry JM et al (2014) Utility of computed tomography or magnetic resonance imaging evaluation of ventricular morphology in suspected cerebrospinal fluid shunt malfunction. J Neurosurg Pediatr 14:160–166. https://doi.org/10.3171/2014.4.PEDS13451
11. Kurwale NS, Agrawal D (2011) Phase-contrast magnetic resonance imaging of intracranial shunt tube: a valuable adjunct in the diagnosis of ventriculoperitoneal shunt malfunction. Clin Neurosurg 58:138–142. https://doi.org/10.1227/neu.0b013e31822784cf
12. Wallace AN, McConathy J, Menias CO et al (2014) Imaging evaluation of CSF shunts. AJR 202:38–53. https://doi.org/10.2214/AJR.12.10270
13. O'Neill BR, Pruthi S, Bains H et al (2013) Rapid sequence magnetic resonance imaging in the assessment of children with hydrocephalus. World Neurosurg 80(6):e307–e312. https://doi.org/10.1016/j.wneu.2012.10.066
14. Patel DM, Tubbs RS, Pate G et al (2014) Fast-sequence MRI studies for surveillance imaging in pediatric hydrocephalus. J Neurosurg Pediatrics 13:440–447. https://doi.org/10.3171/2014.1.PEDS13447
15. Tekes A, Senglaub SS, Ahn ES et al (2018) Ultrafast brain MRI can be used for indications beyond shunted hydrocephalus in pediatric patients. AJNR 39:1515–1518. https://doi.org/10.3174/ajnr.A5724
16. Elkafrawy F, Reda I, Elsirafy M et al (2017) Three-dimensional constructive interference in steady state sequences and phase-contrast magnetic resonance imaging of arrested hydrocephalus. World Neurosurg 98:296–302. https://doi.org/10.1016/j.wneu.2016.10.140
17. Mohammad SA, Osman NM, Khalil RM (2018) Phase-contrast and three-dimensional driven equilibrium (3D-DRIVE) sequences in the assessment of paediatric obstructive hydrocephalus. Childs Nerv Syst 34:2223–2231. https://doi.org/10.1007/s00381-018-3850-6
18. Mohammad SA, Osman NM, Ahmed KA (2019) The value of CSF flow studies in the management of CSF disorders in children: a pictorial review. Insights Imaging 10:1–13. https://doi.org/10.1186/s13244-019-0686-x
19. Chiewvit S, Nuntaaree S, Kanchaanapiboon P et al (2014) Assessment lumboperitoneal or ventriculoperitoneal shunt patency by radionuclide technique: a review experience cases. World J Nucl Med 13:75–84. https://doi.org/10.4103/1450-1147.139135
20. Jayanth A, Benabbas R, Chao J et al (2021) Diagnostic modalities to determine ventriculoperitoneal shunt malfunction: a systematic review and meta-analysis. Am J Emerg Med 39:180–189. https://doi.org/10.1016/j.ajem.2020.09.024
21. Zhang H, Zhang J, Peng J et al (2019) The diagnosis of ventriculoperitoneal shunt malfunction by using phase-contrast cine magnetic resonance imaging. J Clin Neurosci 64:141–144. https://doi.org/10.1016/j.jocn.2019.03.033
22. Martínez-Lage JF, López-Guerrero AL, Almagro M (2015) Clinical manifestations of CSF shunt complications. In: Rocco CD, Turgut M, Jallo G, et al. editors. Complications of CSF shunting in hydrocephalus. P13–32. Springer, Cham. https://doi.org/10.1007/978-3-319-09961-3_2
23. Albugami SM, Alwadi KW, Alrugaib AK, et al (2021) Prevalence and characteristics of shunt malfunction without ventricular size change at King Abdulaziz Medical City in Riyadh. Neurosciences 26:31–35. https://doi.org/10.17712/nsj.2021.1.20200099
24. Reynolds RA, Ahluwalia R, Krishnan V et al (2021) Risk factors for unchanged ventricles during pediatric shunt malfunction. JNS 28:703–709. https://doi.org/10.3171/2021.6.PEDS2125
25. Paff M, Alexandru-Abrams D, Muhonen M et al (2018) Ventriculoperitoneal shunt complications: a review. Interdiscip Neurosurg 13:66–70. https://doi.org/10.1016/j.inat.2018.04.004
26. Pettorini B, Frassanito P, Tamburrini G et al (2008) Retrieval of ventricular catheter with the aid of endoscopy Technical note. J Neurosurg Pediatr 2:71–74. https://doi.org/10.3171/PED/2008/2/7/071
27. Dickerman RD, McConathy WJ, Do JM et al (2005) Failure rate of frontal versus parietal approaches for proximal catheter placement in ventriculoperitonal shunts: revisited. J Clin Neurosci 12:781–783. https://doi.org/10.1016/j.jocn.2004.12.005
28. Dobran M, Nasi D, Mancini F et al (2018) Relationship between the location of the ventricular catheter tip and the ventriculoperitoneal shunt malfunction. Clin Neurol Neurosurg 175:50–53. https://doi.org/10.1016/j.clineuro.2018.10.006
29. Huisman TA (2005) Intracranial hemorrhage: ultrasound, CT and MRI findings. Eur Radiol 15:434–440. https://doi.org/10.1007/s00330-004-2615-7
30. Wei Q, Xu Y, Peng K et al (2018) Value of the application of neuroendoscope in the treatment of ventriculoperitoneal shunt blockage. World Neurosurg 116:e469–e475. https://doi.org/10.1016/j.wneu.2018.05.007
31. Pontes JP, Ferreira-Pinto PH, Simoes EL et al (2021) Removal of the retained ventricular catheter using the endoscopic monopolar instrument. Case Rep Surg. https://doi.org/10.1155/2021/2880979
32. Khalatbari H, Parisi MT (2021) Management of hydrocephalus in children: anatomic imaging appearances of CSF shunts and their complications. AJR 216:187–199. https://doi.org/10.2214/AJR.20.22888
33. Tsitouras V, Sgouros S (2015) Mechanical complications of shunts. In: Rocco CD, Turgut M, Jallo G, et al.(eds) Complications of CSF shunting in hydrocephalus. P129–140, Springer, Cham. https://doi.org/10.1007/978-3-319-09961-3_8
34. Hanaka BW, Bonowa RH, Harrisb CA et al (2017) Cerebrospinal fluid shunting complications in children. Pediatr Neurosurg 52:381–400. https://doi.org/10.1159/000452840

35. Desai KR, Babb JS, Amodio JB (2007) The utility of the plain radiograph "shunt series" in the evaluation of suspected ventriculoperitoneal shunt failure in pediatric patients. Pediatr Radiol 37:452–456. https://doi.org/10.1007/s00247-007-0431-3
36. Griffey RT, Ledbetter S, Khorasani R (2007) Yield and utility of radiographic "shunt series" in the evaluation of ventriculo-peritoneal shunt malfunction in adult emergency patients. Emerg Radiol 13:307–311. https://doi.org/10.1007/s10140-006-0557-x
37. Goeser CD, McLeary MS, Young LW (1998) Diagnostic imaging of ventriculoperitoneal shunt malfunctions and complications. Radiographics 18:635–651. https://doi.org/10.1148/radiographics.18.3.9599388
38. Chung JJ, Yu JS, Kim JH et al (2009) Intraabdominal complications secondary to ventriculoperitoneal shunts: CT findings and review of the literature. AJR 193:1311–1317. https://doi.org/10.2214/AJR.09.2463
39. Agarwal N, Shukla RM, Agarwal D et al (2017) Pediatric ventriculoperitoneal shunts and their complications: an analysis. J Indian Assoc Pediatr Surg 22:155–157. https://doi.org/10.4103/0971-9261.207624
40. Kalra S, Shah K, Tyagi S et al (2022) An indigenous method of securing ventriculoperitoneal shunt tube in peritoneal cavity. Indian J Neurosurg 11:30–32. https://doi.org/10.1055/s-0041-1722826
41. DiLuna ML, Johnson MH, Bi WL et al (2006) Sterile ascites from a ventriculoperitoneal shunt: a case report and review of the literature. Childs Nerv Syst 22:1187–1193. https://doi.org/10.1007/s00381-006-0054-2
42. Johnson JA, O'Halloran PJ, Crimmins D et al (2016) Thinking outside the shunt—sterile CSF malabsorption in pilocytic astrocytomas: case series and review of the literature. Childs Nerv Syst 32:2255–2260. https://doi.org/10.1007/s00381-016-3112-4
43. Balakrishnan V, Jeanmonod R (2014) Two episodes of ventriculoperitoneal shunt migration in a patient with idiopathic intracranial hypertension. Case Rep Emerg Med 2014. https://doi.org/10.1155/2014/280793
44. Morrison JF, Sung KE, Bergman AM et al (2010) A novel solution to reduce the complications of distal shunt catheter displacement associated with obesity. J Neurosurg 113:1314–1316. https://doi.org/10.3171/2010.6.JNS10300
45. Nagasaka T, Inao S, Ikeda H et al (2010) Subcutaneous migration of distal ventriculoperitoneal shunt catheter caused by abdominal fat pad shift—three case reports. Neurol Med Chir (Tokyo) 50:80–82. https://doi.org/10.2176/nmc.50.80
46. Chatterjee S, Harischandra L (2018) Cerebrospinal fluid shunts—how they work: the basics. J Neurology India 66:24–35. https://doi.org/10.4103/0028-3886.222820
47. Swoboda M, Hochman MG, Fritz JS, et al (Accessed: 20-Nov-2021) A new method for CSF shunt patency assessment. Neurodx.com. [Online]. https://neurodx.com/wp-content/uploads/2017/10/Swoboda2013-A-new-method-for-CSF-shunt-patency-assessment.pdf
48. Khalatbari H, Parisi MT (2020) Complications of CSF shunts in pediatrics: functional assessment with CSF shunt scintigraphy—performance and interpretation. AJR 215:1474–1489. https://doi.org/10.2214/AJR.20.22899

Publisher's Note